Decoupling conservative forces and hydrodynamic interactions between optically trapped spheres

Roman Kreiserman,[1,2] Omri Malik,[2,3] and Ariel Kaplan[2,3,*]

[1]*Faculty of Physics, Technion–Israel Institute of Technology, Haifa 32000, Israel*
[2]*Faculty of Biology, Technion–Israel Institute of Technology, Haifa 32000, Israel*
[3]*Russell Berrie Nanotechnology Institute, Technion–Israel Institute of Technology, Haifa 32000, Israel*

Characterizing the interactions between colloidal particles is important, both from a fundamental perspective as well as due to its technological importance. However, current methods to measure the interaction forces between two colloids have significant limitations. Here we describe a method that exploits the fluctuation spectra of two optically trapped microspheres in order to extract, and decouple, the conservative forces acting between them and their hydrodynamic coupling. We demonstrate the proposed method with two silica microspheres, and find good agreement between our results and previous predictions for the hydrodynamic and electrostatic interactions between the spheres.

I. INTRODUCTION

Pairwise interactions between particles determine the collective behavior of multiparticle systems. In the case of suspended colloidal particles, these interactions are involved in a variety of natural phenomena, such as sedimentation [1], aggregation [2], and the formation of colloidal crystals [3,4], as well as in industrial processes, from food technology [5] to pharmaceutical research [6]. Hydrodynamic interactions between micron-sized particles moving in a fluid affect the behavior of microfluidic devices [7–9] and biological systems [10]. In addition, colloidal systems play an important role also as a model for other physical phenomena such as phase transitions [11], and multibody interactions [12,13]. As a result, characterizing the nature and magnitude of these interaction forces is of great interest.

Different methods have been used to characterize surface forces and hydrodynamic interactions between colloidal particles, or between a colloid and a wall. Video microscopy [14–21] and scattering from the evanescent field of a total internal reflection microscope [22–25] were used to monitor the motion of freely diffusing colloids [14–18] or colloids initially positioned and then release by an optical trap [19–21,23–25]. The shift in mean position of an optically trapped colloid was used to directly measure the forces between the trapped particle and a second particle held by a micropipette [26]. The resolution of these camera-based methods is limited by the pixel size, and forces can be measured only at relatively large distances because of image analysis limitations [27]. Other researchers used the colloidal probe technique, based on an atomic force microscope (AFM) cantilever with a microsphere attached to its tip, that is brought into the proximity of a surface [28,29], or a second microsphere deposited on a surface [30–32]. A limitation of this method arises from the high stiffness of AFM cantilevers that

limits the measurement range to high forces. Moreover, the cantilever is relatively large and brought to the surface at high speed, resulting in significant hydrodynamic perturbations. Notably, the fluctuation spectrum of a harmonically trapped colloid was shown to be a sensitive probe of additional forces acting on the particle, and previous works exploited the fluctuation spectra of colloids held by optical traps to characterize the hydrodynamic coupling between them [33,34], and to measure the interaction forces between a trapped colloid and a surface [35]. However, more work was required to find a reliable and accurate method to simultaneously measure the hydrodynamic and conservative interactions between two suspended spheres. In this paper, we present and demonstrate such a method, based on the analysis of the coupled fluctuations of two microspheres trapped in optical traps.

II. RESULTS AND DISCUSSION

The motion of an optically trapped microsphere in the small Reynolds numbers regime can be described by a Langevin equation, $\gamma_0 \dot{x}_{sphere} + \kappa_{OT} x_{sphere} = f_T(t)$, where x_{sphere} is the instantaneous position of the particle, γ_0 its drag coefficient, and κ_{OT} the stiffness or spring constant of the harmonic trapping potential. $f_T(t)$ represents the random thermal forces acting on the particle, which are assumed to have zero mean and no memory, i.e., $f_T(t) = 0$ and $f_T(t)f_T(t') = 2\gamma_0 k_B T \delta(t - t')$. The power spectrum density that corresponds to this equation of motion has the shape of a Lorentzian,

$$P(f) \triangleq |\tilde{x}(f)|^2 = \frac{D_0}{\pi^2 (f^2 + f_c^2)}, \tag{1}$$

where $D_0 = k_B T / \gamma_0$ is the diffusion coefficient of the sphere and $f_c = \kappa_{OT}/2\pi\gamma_0$ is the "corner frequency," which represents the crossover between a constant power at low frequencies and a power that scales as f^{-2} for high frequencies, which are insensitive to the trapping potential. This well-characterized spectral dependence of the fluctuations is
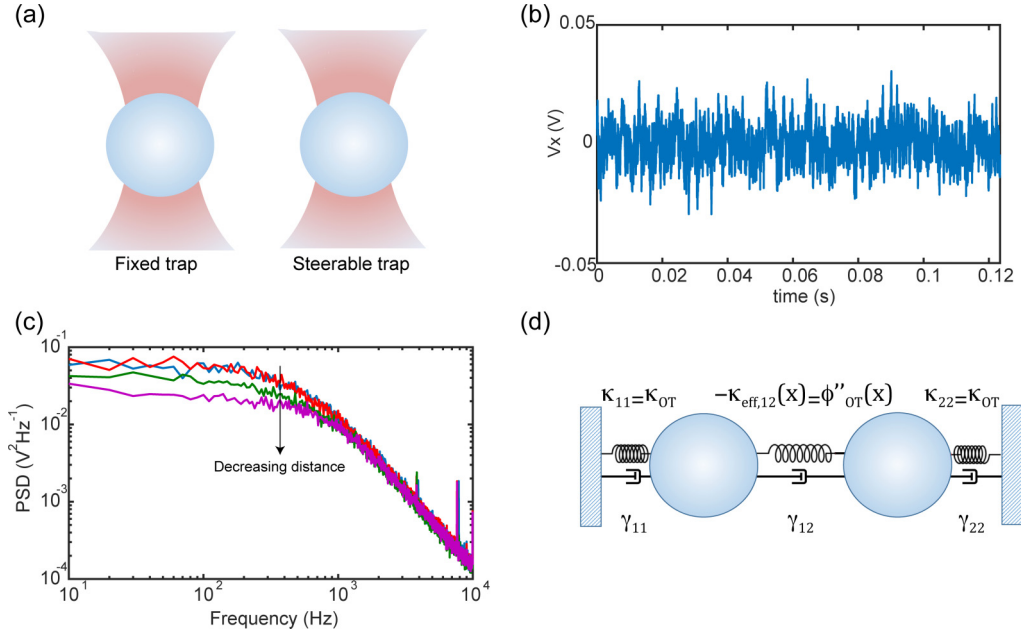
*akaplanz@technion.ac.il

FIG. 1. Modeling the interaction between two suspended colloids. (a) Two $\sim$2-um silica microspheres are trapped with two optical traps positioned at a constant distance. (b) The instantaneous position of the microspheres is determined by back focal plane interferometry, sampling the voltage signals of a position sensitive detector at 81 kHz. Shown is the signal corresponding to the horizontal movement of one of the microspheres. (c) Power spectral density (PSD) for the position fluctuations of one of the spheres, as derived from the sampled signals, for different mean distances between the two spheres (distance between the surface of the beads: 2800, 1600, 400, and 290 nm). (d) A model for the motion of the microspheres includes the trap's harmonic potential and each sphere's drag coefficient, and also an effective pairwise interaction potential and hydrodynamic coupling between the spheres.

the basis for the calibration of optical tweezers: If the drag coefficient is known, for example, by applying the Stokes law $\gamma_0 = 6\pi\eta R_{\text{sphere}}$ where η is the medium's viscosity and R_{sphere} the diameter of the sphere, determining f_c is enough to calculate κ_{OT}. Alternatively, applying an additional, sinusoidal driving force of known amplitude and measuring the size of the additional peak in the spectrum enables determining both γ_0 and κ_{OT} simultaneously [36].

We follow the fluctuations of two identical 2-μm silica beads [Fig. 1(a)], using a dual-trap optical tweezers setup as previously described [37,38], but using two separate lasers to minimize interference at short distances. Briefly, the collimated beams ($w_0 = 4$ mm) from two fiber-coupled lasers (852.2 and 855.2 nm; TA PRO, Toptica) were directed to two separate mirrors, one of which is mounted on a nanometer scale mirror mount (Nano-MTA, Mad City Labs), and combined with a polarizing beam splitter (PBS). An X2 telescope expands the beam, and also images the plane of the mirrors into the back focal plane of the focusing microscope objective (Nikon, Plan Apo VC 60X, NA/1.2), ensuring that steering will not result in shifting from the objective aperture. Two optical traps are formed at the objective's focal plane, each by a different laser. The light is collected by a second, identical objective, the two beams separated by a PBS and imaged onto two position sensitive detectors (First Sensor, DL100-7PCBA3). The position of the beads relative to the center of the trap is determined by a back focal plane interferometer [39], sampling the detectors' signals at 81 kHz [Fig. 1(b)].

The fluctuations of the beads were recorded, first for an isolated bead (i.e., in the absence of a second bead), and then when both beads were trapped (see Supplemental Material

[40] for a detailed description of the experimental protocol). The presence of a second bead [Fig. 1(c)] significantly affects the spectrum in a distance-dependent manner, indicating the existence of interactions between the beads. Moreover, the perturbation of the spectra indicates that the microspheres' motion is not fully described by the Langevin equation presented above, and therefore the use of the spectra to calibrate the optical traps is not straightforward. However, it also suggests that the spectra contain information about the nature of these interactions, which might be accessed by properly analyzing both microspheres' fluctuations.

In order to extract information on the interactions between the spheres, we formulate a simple model for their motion, considering two optically trapped spheres that interact, both hydrodynamically and by conservative forces between them [Fig. 1(d)]. The hydrodynamic interaction between the spheres is modeled by a damper connecting them. Static, conservative forces between the spheres are modeled as a spring connecting both spheres, whose stiffness is equal to the second derivative of the interaction potential. (For simplicity, we limit our discussion to the movement of the spheres in the lateral direction perpendicular to the line connecting the centers of the spheres). The equation of motion of the spheres is now a *coupled* Langevin equation,

$$
\begin{pmatrix} \gamma_{11} & \gamma_{12} \\ \gamma_{21} & \gamma_{22} \end{pmatrix} \begin{pmatrix} \dot{x}_1 \\ \dot{x}_2 \end{pmatrix} + \begin{pmatrix} \kappa_{\text{eff},11} & -\kappa_{\text{eff},12} \\ -\kappa_{\text{eff},21} & \kappa_{\text{eff},22} \end{pmatrix} \begin{pmatrix} x_1 \\ x_2 \end{pmatrix}
$$
$$
= \begin{pmatrix} f_{T,1}(t) \\ f_{T,2}(t) \end{pmatrix}, \tag{2}
$$

which can also be written as $\Gamma \dot{X} + K X = F_T(t)$. The drag (or Oseen) tensor Γ, includes in its diagonal terms γ_{ii} the friction associated with the motion of the individual particle, i.e., the local drag coefficient of an individual sphere, and in the off-diagonal terms, $\gamma_{ij,i\neq j}$, the friction associated with the relative motion of the two spheres, i.e., the hydrodynamic coupling between the spheres that arises from the fluid flow generated by their movement. From symmetry considerations $\gamma_{12} = \gamma_{21}$, and in the case of two identical spheres, $\gamma_{11} = \gamma_{22}$ (see Supplemental Material [40] for a discussion of the case of spheres of different sizes). Off-diagonal terms in the stiffness tensor, K, describe any existing conservative force between the spheres $[F = \phi'(x)$, where $\phi(x)$ is the interaction potential], and diagonal terms include also the stiffness of the optical trap:

$$K = \begin{pmatrix} \kappa_{\mathrm{OT}} + \phi''(x) & \phi''(x) \\ \phi''(x) & \kappa_{\mathrm{OT}} + \phi''(x) \end{pmatrix}. \qquad (3)$$

On the right-hand side of Eq. (2) is the random Brownian force acting on each of the spheres, which, as before, is described by its two moments: $\langle f_{T,i}(t) \rangle = 0$ and $\langle f_{T,i}(t) f_{T,j}(t') \rangle = 2\gamma_{ij} k_B T \delta(t - t')$ for $i, j \in \{1, 2\}$. Similarly to Refs. [34,41,42], we decouple the coupled Langevin equation by defining center-of-mass coordinates: $X_s = (x_1 + x_2)/\sqrt{2}$ and $X_{as} = (x_1 - x_2)/\sqrt{2}$. These new coordinates result in two *independent* Langevin equations,

$$\gamma_s \dot{X}_s + \kappa_s X_s = f_{T,s}(t), \qquad (4)$$

and

$$\gamma_{as} \dot{X}_{as} + \kappa_{as} X_{as} = f_{T,as}(t), \qquad (5)$$

where we have defined $\gamma_s = \gamma_{11} + \gamma_{12}$, $\gamma_{as} = \gamma_{11} - \gamma_{12}$, $\kappa_s = \kappa_{\mathrm{eff},11} - \kappa_{\mathrm{eff},12}$, and $\kappa_{as} = \kappa_{\mathrm{eff},11} + \kappa_{\mathrm{eff},12}$. In terms of this new coordinate system, the Langevin equations describe the symmetric motion of the center of mass, X_s, where both spheres move in phase maintaining a constant separation, and the antisymmetric, relative motion of the two spheres, X_{as}, where the spheres move out of phase stretching or compressing the spring tethering them [Fig. 1(d)]. γ_s, γ_{as} are the drag coefficient, and κ_s, κ_{as} the effective trap stiffness, for the symmetric and antisymmetric movements, respectively. The corresponding power spectrum densities are given by

$$P_s(f) = 4 \int_0^\infty X_s^2(t) \cos(2\pi f t) dt = \frac{k_B T}{\pi^2 \gamma_s (f^2 + f_{c,s}^2)}, \qquad (6)$$

and

$$P_{as}(f) = 4 \int_0^\infty X_{as}^2(t) \cos(2\pi f t) dt = \frac{k_B T}{\pi^2 \gamma_{as} (f^2 + f_{c,as}^2)}, \qquad (7)$$

where we have used the definition $f_{c,k} = \kappa_k / 2\pi \gamma_k$ for $k \in \{s, as\}$. Similarly to the case of a single sphere in a single

optical trap, the resulting power spectra for the symmetric and antisymmetric motion of the interacting spheres are both Lorentzians. By fitting the experimentally measured power spectra to the expressions above, one can deduce γ_s, γ_{as}, κ_s, and κ_{as}. Then, the drag coefficients and effective stiffness in the original coordinates can be found by transforming the coordinates back, i.e., $\gamma_{11} = (\gamma_s + \gamma_{as})/2$, $\gamma_{12} = (\gamma_s - \gamma_{as})/2$, $\kappa_{\mathrm{eff},11} = (\kappa_s + \kappa_{as})/2$ and $\kappa_{\mathrm{eff},12} = (\kappa_{as} - \kappa_s)/2$.

The process described above can be repeated for different (mean) distances between the spheres, providing the functional dependence of the hydrodynamic coupling, $\gamma_{12}(x)$, on the distance between the beads. Moreover, from the distance-dependent $\kappa_{\mathrm{eff}}(x)$, it is possible to find $\phi''(x)$ by subtracting the value of the trap stiffness in the absence of an interaction, i.e., when the particles are far away, or when only one particle is present at a time, $\phi''(x) = \kappa_{\mathrm{eff}}(x) - \kappa_{\mathrm{OT}}$. Finally, similarly to Ref. [35], integration of $\phi''(x)$ yields the static force:

$$F(x) = -\phi'(x) = -\int_0^x \phi''(\tilde{x}) d\tilde{x}. \qquad (8)$$

The method described above was used to characterize the interactions between the two silica beads. We calculated the symmetric and antisymmetric power spectra [Figs. 2(a) and 2(b)] and, by fitting them to Lorenzian functions, the drag coefficients [Fig. 2(c)] and effective spring constants [Figs. 2(d)] associated with the symmetric and antisymmetric dynamics. As expected, the asymmetric drag coefficient grows as the distance between the spheres diminishes, reflecting the increasing difficulty of squeezing the fluid amidst the gap between the two spheres as they become closer. More surprisingly, the symmetric drag coefficient shows a slight decrease at small separations. This may arise from the fact that, at separations smaller than the radius of the spheres, their in-phase motion appears like the effective movement of a single elongated object, whose drag coefficient is smaller than that of two separated spheres. The stiffness for the symmetric movement [Fig. 2(c)] remains constant and equal to the trap's stiffness, matching the value from the theoretical derivation above, since the effective spring coupling the spheres [Fig. 1(d)] is unperturbed when both spheres move in phase. In contrast, the asymmetric stiffness is equal to the optical trap stiffness at large separations but grows as the spheres approach each other, indicating the existence of a repulsive force (i.e., an effective spring) between them. This is also evident when the coupling spring effective stiffness, $\kappa_{\mathrm{eff, 12}}$, is calculated from the difference between κ_s and κ_{as} [Fig. 2(e)]: at large separations, the effective stiffness of each sphere is equal to the stiffness of the optical trap, since the optical force is the only force acting on each sphere. As the distance between the spheres reduces to a distance of 100 nm and less, the repulsive force between them results in an increase in the effective stiffness.

As a validation for our method, we measured the axial and perpendicular drag coefficient for spheres submerged in water, as a function of their separation (Fig. 3). A number of theoretical predictions for the hydrodynamic interactions between spheres exists in the literature. Solutions for widely separated spheres include those using reflections [43], bispherical coordinates [44], tangent-sphere coordinates [45], collocation methods [46], and the method of reflections
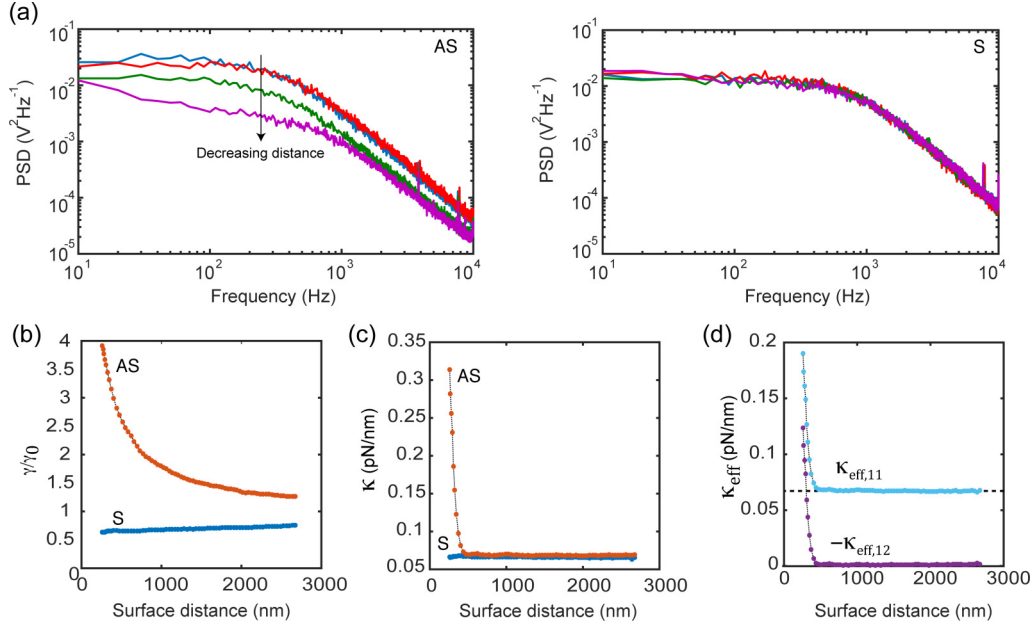
FIG. 2. (a) Calculated power spectrum density for the fluctuations in the asymmetric (left) and symmetric (right) motion of the spheres for the different mean distances between the spheres as indicated in Fig. 1. (b) Drag coefficients for the symmetric (bottom) and asymmetric (top) modes of motion. (c) Spring stiffness for the symmetric (bottom) and asymmetric (top) modes of motion. (d) Effective spring stiffness as a function of the separation between the spheres.

combined with asymptotic methods [47]. For spheres in close proximity, there is only one theoretical derivation, by Jefferey and Onishi [47], using a method of reflections with asymptotic methods (see Supplemental Material [40] for a discussion of these methods and their theoretical predictions). Without any fitting parameters, we observed excellent agreement with the theoretical hydrodynamic result at all separation distances.

To further test the performance of the method, we measured the force between the negatively charged silica microspheres in NaCl solutions of different concentrations [Fig. 4(a)]. Such force profiles can be described by the Derjaguin-Landau-Verwey-Overbeek (DLVO) theory, which combines the effects of the van der Waals (VDW) attraction and the electrostatic repulsion due to the "double layer" of

counterions. For two spheres,

$$\frac{F(r)}{R_c} = 4\pi \varepsilon_W \varepsilon_0 \psi_s^2 e^{-\frac{r}{L_D}} - \frac{H}{12}\frac{1}{r^2}, \tag{9}$$

where $F(r)$ is the force between two spheres, of radius R_a and R_b, at a distance r between their centers; ε_0 is the vacuum permittivity; ε_W the dielectric constant of water; ψ_s the surface potential; L_D the Debye length; H the Hamaker constant; and we have defined an "effective" radius" $R_c = R_a R_b / (R_a + R_b)$. Since VDW forces contribute only at relatively high salt concentrations (>1 M NaCl) and at small surface separations (<10 nm) [48], they can be neglected in our case. As expected, Fig. 4(a) shows an exponential dependence on the sphere-to-sphere distance for all measured salt
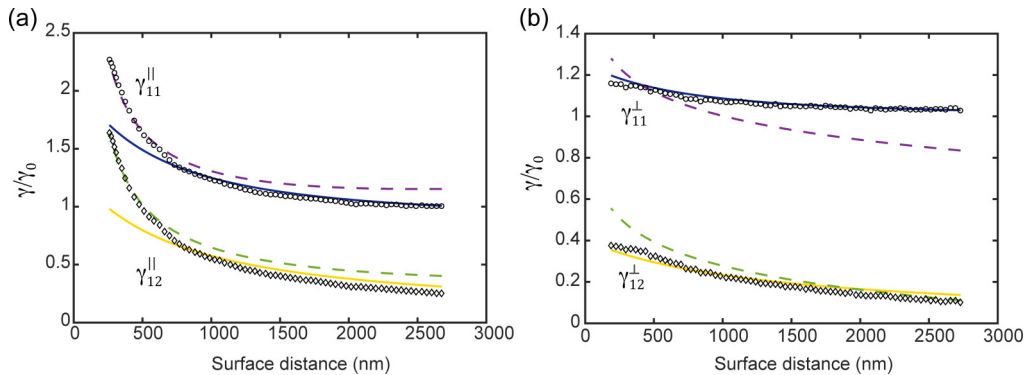

FIG. 3. Measurements of the hydrodynamic interactions between the spheres, depicted as corrections for the drag coefficient as a function of the spheres' separation. (a) Parallel (lateral) drag coefficient for the self (top) and mutual (bottom) drag coefficient. (b) Perpendicular (axial) drag coefficient for the self (top) and mutual drag coefficient. Solid lines show the predictions of a theoretical model for long-range interactions (Eqs. (14)–(17) in the Supplemental Material [40]), while dashed lines show those of a theoretical model for short-range interaction (Eqs. (18)–(21) in the Supplemental Material [40]).
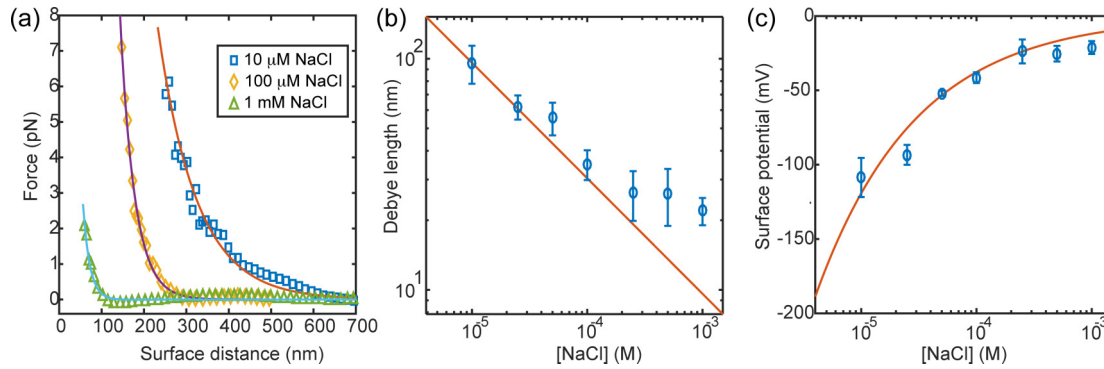
FIG. 4. (a) Conservative force between the spheres, as a function of the distance between their surfaces, for [NaCl] $= 10\,\mu M$ (squares), $100\,\mu M$ (diamonds), and 1 mM (triangles). Solid lines are fits to Eq. (9), with two fitting parameters: the Debye length and the Gouy-Chapman surface potential. (b) The Debye length as a function of the ionic strength, as determined from the fit to the measured force profile. The solid line depicts the calculated Debye length [Eq. (10)]. (c) The electrostatic surface potential as function of the ionic strength. The solid line is based on the Gouy-Chapman model [Eq. (11)] with a single fitting parameter, the surface charge density, which was found to be $\sigma = 8.8 \times 10^{-14}$ C.

concentrations. Fitting the force profiles with the exponential part of Eq. (9) yields the Debye length, L_D, and the surface potential, ψ_s. At intermediate salt concentrations (expressed in molar units), L_D (in nm) is well described by the expression

$$L_D = 0.304/[\text{NaCl}]^{-1/2}, \qquad (10)$$

as expected for a monovalent electrolyte solution at room temperature [49] [(Fig. 4(b)]. However, at high salt concentration, we observe a large deviation from this dependence, in agreement with previous reports [50–52]. Another deviation was observed for pure water, whose measured Debye length is substantially smaller than expected, possibly due to impurities [21,35]. Figure 4(c) shows the dependence of the surface potentials on [NaCl], where a negative sign is assigned to match the negative net charge of silica at pH > 2.5 [53]. The ionic strength dependence is described well with the Gouy-Chapman equation, which relates the surface charge density σ and the diffuse layer potential ψ_s for an isolated charged interface:

$$\psi_s = \frac{2k_B T}{e}\,\text{arcsinh}\left(\frac{e\sigma L_D}{2k_B T \varepsilon_W \varepsilon_0}\right). \qquad (11)$$

When this equation was fitted to the data, with σ as the fitting parameter, we found $\sigma = 8.8 \times 10^{-14}$ C, which is

reasonable for SiO_2 at neutral pH conditions, as found by other techniques [23,31,54]. Of note, as expected given the coefficients of the Jones-Dole equation for NaCl and the range of concentrations used in our experiments [55], the presence of the salt did not affect the estimated bulk drag coefficient (see Supplemental Fig. 1 [40]).

In summary, we presented and experimentally demonstrated a method that enables extracting, and decoupling, the conservative forces and hydrodynamic interactions between two optically trapped colloidal spheres. We validated our proposed method, by measuring the hydrodynamic interactions between two microspheres, as a function of their distance, and the double layer electrical forces between them as a function of the salt concentration. Excellent agreement with the relevant theories was found in both cases. Beyond its potential as a useful tool in colloid science and applications, our method paves the way for the characterization of close-range biophysical processes, such as membrane-membrane interactions.

[1] J. Palacci, C. Cottin-Bizonne, C. Ybert, and L. Bocquet, Phys. Rev. Lett. **105**, 088304 (2010).

[2] N. M. Kovalchuk and V. M. Starov, Adv. Colloid Interface Sci. **179–182**, 99 (2012).

[3] P. J. Lu and D. A. Weitz, Annu. Rev. Condens. Matter Phys. **4**, 217 (2013).

[4] J. Dobnikar, Y. Chen, R. Rzehak, and H. H. von Grünberg, J. Chem. Phys. **119**, 4971 (2003).

[5] E. Dickinson, Annu. Rev. Food Sci. Technol **6**, 211 (2015).

[6] H. Ohshima and K. Makino, *Colloid and Interface Science in Pharmaceutical Research and Development* (Elsevier, Amsterdam, 2014).

[7] K. Misiunas, S. Pagliara, E. Lauga, J. R. Lister, and U. F. Keyser, Phys. Rev. Lett. **115**, 038301 (2015).

[8] B. Cui, H. Diamant, B. Lin, and S. A. Rice, Phys. Rev. Lett. **92**, 258301 (2004).

[9] X. Xu, S. A. Rice, B. Lin, and H. Diamant, Phys. Rev. Lett. **95**, 158301 (2005).

[10] J. Lebowitz, M. S. Lewis, and P. Schuck, Protein Sci. **11**, 2067 (2009).

[11] B. Li, D. Zhou, and Y. Han, Nat. Rev. Mater. **1**, 15011 (2016).

[12] J. J. Gray, B. Chiang, and R. T. Bonnecaze, Nature **402**, 750 (1999).

[13] G. Pandav, V. Pryamitsyn, J. Errington, and V. Ganesan, J. Phys. Chem. B **119**, 14536 (2015).

[14] K. Vondermassen, J. Bongers, A. Mueller, and H. Versmold, Langmuir **10**, 1351 (1994).

[15] G. M. Kepler and S. Fraden, Phys. Rev. Lett. **73**, 356 (1994).

[16] M. D. Carbajal-Tinoco, F. Castro-Román, and J. L. Arauz-Lara, Phys. Rev. E **53**, 3745 (1996).

[17] M. D. Carbajal-Tinoco, R. Lopez-Fernandez, and J. L. Arauz-Lara, Phys. Rev. Lett. **99**, 138303 (2007).

[18] S. H. Behrens and D. G. Grier, Phys. Rev. E **64**, 050401 (2001).

[19] J. C. Crocker and D. G. Grier, Phys. Rev. Lett. **73**, 352 (1994).

[20] J. C. Crocker, J. Chem. Phys. **106**, 2837 (1997).

[21] P. M. Hansen, J. K. Dreyer, J. Ferkinghoff-Borg, and L. Oddershede, J. Colloid Interface Sci. **287**, 561 (2005).

[22] D. C. Prieve, Adv. Colloid Interface Sci. **82**, 93 (1999).

[23] A. R. Clapp and R. B. Dickinson, Langmuir **17**, 2182 (2001).

[24] T. Ota, T. Sugiura, and S. Kawata, Appl. Phys. Lett. **80**, 3448 (2002).

[25] S. H. Behrens, J. Plewa, and D. G. Grier, Eur. Phys. J. E **10**, 115 (2003).

[26] C. Gutsche, U. F. Keyser, K. Kegler, F. Kremer, and P. Linse, Phys. Rev. E **76**, 031403 (2007).

[27] J. Baumgartl and C. Bechinger, Europhys. Lett. **71**, 487 (2005).

[28] G. Toikka and R. A. Hayes, J. Colloid Interface Sci. **191**, 102 (1997).

[29] H. J. Butt, B. Cappella, and M. Kappl, Surf. Sci. Rep. **59**, 1 (2005).

[30] F. J. M. Ruiz-Cabello, P. Maroni, and M. Borkovec, J. Chem. Phys. **138**, 234705(2013).

[31] M. Elzbieciak-Wodka, M. N. Popescu, F. J. M. Ruiz-Cabello, G. Trefalt, P. Maroni, and M. Borkovec, J. Chem. Phys. **140**, 104906(2014).

[32] M. Radiom, B. Robbins, M. Paul, and W. Ducker, Phys. Fluids **27**, 022002 (2015).

[33] J.-C. Meiners and S. R. Quake, Phys. Rev. Lett. **82**, 2211 (1999).

[34] S. Henderson, S. Mitchell, and P. Bartlett, Phys. Rev. E **64**, 061403 (2001).

[35] E. Schäffer, S. F. Nørrelykke, and J. Howard, Langmuir **23**, 3654 (2007).

[36] S. F. Tolic-Nørrelykke, E. Schäffer, J. Howard, F. S. Pavone, F. Jülicher, and H. Flyvbjerg, Rev. Sci. Instrum. **77**, 103101 (2006).

[37] O. Malik, H. Khamis, S. Rudnizky, A. Marx, and A. Kaplan, Nucleic Acids Res. **45**, 10190 (2017).

[38] O. Malik, H. Khamis, S. Rudnizky, and A. Kaplan, Nucleic Acids Res. **45**, 12954 (2017).

[39] F. Gittes and C. F. Schmidt, Opt. Lett. **23**, 7 (1998).

[40] See Supplemental Material at http://link.aps.org/supplemental/10.1103/PhysRevE.99.012611 for a discussion of spheres of different sizes, a detailed description of the experimental procedure, and a discussion of the theoretical predictions for the hydrodynamic interactions between two spheres.

[41] J. R. Moffitt, Y. R. Chemla, D. Izhaky, and C. Bustamante, Proc. Natl. Acad. Sci. USA **103**, 9006 (2006).

[42] M. N. Romodina, M. D. Khokhlova, E. V. Lyubin, and A. A. Fedyanin, Sci. Rep. **5**, 10491 (2015).

[43] A. J. Goldman, R. G. Cox, and H. Brenner, Chem. Eng. Sci. **21**, 1151 (1966).

[44] M. E. O'Neill and R. Majumdar, ZAMP **21**, 164 (1970).

[45] M. B. A. Cooley and M. E. O'Neill, Math. Proc. Cambridge Philos. Soc. **66**, 407 (1969).

[46] P. Ganatos, R. Pfeffer, and S. Weinbaum, J. Fluid Mech. **84**, 79 (1978).

[47] D. J. Jeffrey and Y. Onishi, J. Fluid Mech. **139**, 261 (1984).

[48] H.-J. Butt and M. Kappl, *Surface and Interfacial Forces* (Wiley-VCH Verlag GmbH & Co. KGaA, Weinheim, Germany, 2010).

[49] J. Israelachvili, *Intermolecular and Surface Forces*, 3rd ed. (Academic Press Inc., New York, 2011).

[50] G. Vigil, Z. Xu, S. Steinberg, and J. Israelachvili, J. Colloid Interface Sci. **165**, 367 (1994).

[51] M. Boström, D. R. M. Williams, and B. W. Ninham, Phys. Rev. Lett. **87**, 168103 (2001).

[52] M. Boström, V. Deniz, G. V. Franks, and B. W. Ninham, Adv. Colloid Interface Sci. **123–126**, 5 (2006).

[53] P. R. Johnson and M. Elimelech, Langmuir **11**, 801 (1995).

[54] W. A. Ducker, T. J. Senden, and R. M. Pashley, Langmuir **8**, 1831 (1992).

[55] R. Dordick, L. Korson, and W. Drost-Hansen, J. Colloid Interface Sci. **72**, 206 (1979).